CRACK GROWTH ANOMALIES IN HAZ FOR PARENT STEEL P91

JAROSLAV BALÍK[1]*, MILOŠ JANEČEK[2], JOSEF PEŠIČKA[2]

The rate of creep crack growth $\dot{a}$ in the intercritical layer of HAZ for parent steel P91 was measured for a range of loads at 600 °C. The TDCB samples were used, the test times ranging from 19 to 6603 h. The crack tip parameter $C^*(t)$ was calculated using line displacements due to creep, the latter obtained from permanent deflections as corrected on instant plasticity.

For long term tests, relatively high growth rates appear so that no unique asymptotic power law $\dot{a} \propto C^{*\Phi}$ exists for all load regimes. Furthermore, an anomalous range of load dependence on crack initiation times was revealed. An attempt is made to correlate these effects with changes in ductility due to possible re-precipitation during thermomechanical exposition. This suggestion is documented by scanning electron microscopy of fracture surfaces and transmission electron microscopy of the exposed intercritical zone ahead of the crack tip.

K e y w o r d s: steel P91, heat affected zone, creep crack growth, growth initiation times, re-precipitation

ANOMÁLIE RŮSTU TRHLINY V TOZ PRO ZÁKLADNÍ OCEL P91

Pro svary základní oceli P91 byla měřena rychlost růstu $\dot{a}$ creepové trhliny v interkritické vrstvě tepelně ovlivněné zóny (TOZ) při 600 °C a jistém oboru zatížení. Byly užity vzorky TDCB, přičemž zatěžovací parametr $C^*(t)$ byl určen z lineárních dilatací způsobených creepem, jež byly získány z trvalých deformací, korigovaných na „okamžitou" plasticitu.

Pro dlouhodobé testy byly zjištěny relativně vysoké růstové rychlosti, takže neexistuje asymptotický mocninný zákon $\dot{a} \propto C^{*\Phi}$, jenž by byl univerzální pro všechna zatížení. Je proveden pokus korelovat tyto efekty se změnami tažnosti, způsobenými možnou reprecipitací během termomechanické expozice. Tento předpoklad je dokumentován řádkovací elektronovou mikroskopií lomových ploch a transmisní elektronovou mikroskopií interkritické zóny před čelem trhliny.

[1] SVÚM, a.s., Research Centre Běchovice, 190 11 Prague 9, Czech Republic
[2] Department of Metal Physics, Charles University, Ke Karlovu 5, 121 16 Prague 2, Czech Republic
* corresponding author, e-mail: balik@svum.cz

1. Introduction

Modified martensitic chromium steels of about 9–12 wt.% Cr and 0.1–0.2 wt.% C find their most extensive use in the construction of steam power plants. Not only static devices such as pipes and tubes but also turbine components (rotors, blades) are often manufactured from the steels of this class. The low thermal expansion coefficient and high thermal conductivity (as compared to austenite) together with a good creep strength and favourable oxidation resistance enable now the long term service times of the order of 10^5 h at the temperatures up to 600 ℃ [1].

The creep resistance of the material is governed generally by the fracture time. If we define the mean deformation rate $\overline{\dot{\varepsilon}}(T,\sigma)$ over the whole lifetime at a fixed stress, the fracture time is expressed by

$$t(T,\sigma) = \frac{\varepsilon_{\mathrm{f}}(T,\sigma)}{\overline{\dot{\varepsilon}}(T,\sigma)} \tag{1}$$

with a respective ductility in the numerator. The rate of creep deformation is governed by kinetics of dislocation glide and climb and by steady state microstructure as established due to the production and recovery of dislocations. The ductility is mainly governed by damage accumulation, the process involving the subsequent nucleation, growth and coalescence of cavities. The microphysical processes of plastic deformation and cavitation, which develop during the service time, may be therefore roughly related to mean deformation rate and ductility, respectively.

Both creep rate and damage development are essentially influenced by the chemical composition of the steel. The creep resistance of the martensite (ferrite) matrix increases not only due to the solid solution hardening but also owing to the presence of fine particles of second phases. The latter also influence grain boundary sliding and grain boundary migration which, as a rule, are accompanying the plastic deformation at high temperatures. As to damage process, the nucleation rate of cavities is very likely to be enhanced by the stress concentration near the precipitates [2]. Also an influence of the second phase particles on the crack growth rate and coalescence of grain boundary cavities may be expected.

A lot of carbide and carbonitride phases have been reported to be present in the steel of this class [3]: $M_{23}C_6$, M_3C, M_7C_3, M_6C, M_5C_2, M_2X, MX and Laves phases. Typically five or more of these particle types are usually present in a creep resistant steel. A stable dispersion of fine nitrides VN seems to be the most efficient creep-strengthener in P91 steel. Another long term phases such as $(CrFeMo)_{23}C_6$ or Laves phase $(FeCr)_2Mo$ undergo a significant coarsening during thermomechanical exposition what causes a decrease in their creep resistance capacity. Recently revealed degradation effect connected to the complex Z-phase nitride Cr(V,Nb)N is also worth noting [4]. During long term service times, the coarse particles of Z-phase are built up consuming the fine dispersion of the VN-precipitates.

Due to stress concentrations at, e.g., shape notches or material inhomogenities, the cracks may be nucleated in a creeping body. In spite of this, when the cracks are growing sufficiently slowly and the creep damage in the bearing sections remains far below the level of tertiary creep stage, the component can be left in service. As the hardly damaged region spreads from the crack tip zone into the uncracked ligament, the crack growth rate continues to increase up to a critical point in which the rates of both crack growth and external displacements accelerate suddenly. Consequently, the service time may be prolonged over the stage of subcritical growth only. Assuming that the secondary creep rate, as governed by the Norton power law

$$\dot{\varepsilon}_{\mathrm{eq}} = A\sigma_{\mathrm{eq}}^{n}, \tag{2}$$

is extended over the whole specimen and that the crack propagation starts just the crack tip strain reaches the value of an appropriate crack tip ductility $\varepsilon_{\mathrm{f}}^{*}$, the subcritical crack velocity may be estimated [5] as $\dot{a} \propto \varepsilon_{\mathrm{f}}^{*-1} A^{\frac{1}{n+1}} C^{*\frac{n}{n+1}}$. The well-known variable C^{*} comprises all the loading details of the sample and it simply parametrises the asymptotic stress and strain rate fields near the crack tip. Using the scaling law $C^{*} \propto AP^{n+1}$ with load P of the sample, see e.g. [6], one obtains the following relation:

$$\dot{a} \propto \frac{AP^{n}}{\varepsilon_{\mathrm{f}}^{*}} \propto \frac{\dot{\varepsilon}_{r}}{\varepsilon_{\mathrm{f}}^{*}}. \tag{3}$$

A geometrical factor is omitted for simplicity. The reference strain rate equals the creep rate in an uniaxial sample of a "reference" cross section.

Comparing the relations (1) and (3), an obvious analogy between the inverse of the crack growth rate and the uniaxial fracture time can be seen. Nevertheless, some substantial physical differences should be kept in mind. First, the different stress states, for a given equivalent stress, in the uniaxial sample and in the front of the crack tip [7] can induce an appreciable difference in the respective fracture strains. Second, the strain rates appearing in (1) and (3) are not related straightforwardly. The mean strain rate of the uniaxial creep involves all deformation stages (including the tertiary one) which developed in the whole sample under constant stress. In the case of crack growth, however, the tertiary regime, if it exists at all, has to be confined to a crack tip zone. The strain rate appearing in (3) should be therefore related to the secondary creep stage presumably, the strain being accumulated under an increasing stress rate as the crack tip comes up.

Creep properties of the weld joints, i.e., of both weld deposits as well as adjacent zones affected by heat flow (HAZ), can differ substantially from those of base material. The reason is that welding represents itself a very complex metallurgical process involving solidification, solid state phase transformations, heat treatment, residual stress development, and alloying effects [1]. As a rule, the creep lifetime of

cross weldments is limited by the fine grained interface region between HAZ and the base material [8]. (This statement, however, appears to be stress-conditioned: for higher loads and shorter lifetimes, the fracture surface is shifted into the base material.) The peak temperature between Ac_1 and Ac_3 was experienced by the intercritical zone and only a partial austenitization took place here. A mixture of fresh transformation products surrounded by the original (re-tempered) martensite is then formed. Coarse $M_{23}C_6$ carbides have been reported [9] to be present in the intercritical zone in comparison to the parent metal P91.

Although the expression (3) can obviously not predict the value of growth rate with accuracy which is requested by engineers, numerous trends in crack growth rate, as induced by geometry, temperature, load, and microstructural material characteristics, may be estimated. The aim of this work is to measure immediately the crack growth rate in the intercritical layer of HAZ to accomplish the previously published data [10] for base and aged steel P91. Typical service temperature and rather wide range of loads are chosen to discover some structure changes appearing prospectively during long term exposures. The mechanical measurements are accompanied by scanning (SEM) and transmission (TEM) electron microscopy of exposed structures.

2. Experimental and evaluation of data

The base material was supplied by VITKOVICE steelworks and comprises (in weight %): 0.1 C, 0.43 Si, 0.4 Mn, 0.015 P, 0.006 S, 8.5 Cr, 0.88 Mo, 0.1 Ni, 0.1 Nb, 0.23 V, 0.018 Al, 0.045 N. The initial state was prepared by normalization (austenitizing) at 1065 ± 25 ℃ and air cooling, followed by tempering at 745 ± 15 ℃ for 4 h and air cooling again. The side grooved tapered double cantilever beam (TDCB) specimens were machined from a weldment, the channel of critical structure being localized between the sidegrooves. The weldment was prepared by TIG-filling of a slot of size of 10 × 12 mm^2 with the weld metal Thyssen Chromo 9V, followed by post weld heat treatment 755 ℃/2 h. The intercritical zone has been detected employing the hardness profile across the weldment, bearing upon the several times reported coincidence between the hardness minimum and critical structure [9]. The situation of the weld in the TDCB-sample is summarised in Fig. 1.

The creep crack growth tests were conducted by constant load method at 600 ℃, the initial values of stress intensity factors K_i ranging (17.9–58.1) $\mathrm{MN \cdot m^{-3/2}}$. The crack lengths and permanent line displacements were monitored microscopically on the test pieces removed from the machine.The creep crack rate is plotted against the well-proved parameter C^*, which represents an amplitude of the singular crack tip stress and strain rate (HRR, Hutchinson-Rice-Rosengren) fields. Assuming that the steady state creep dominates over the whole sample, the scaling laws [6] lead to the relation $C^* \propto P\dot{\Delta}_\mathrm{c}$ at a fixed geometry. Here, $\dot{\Delta}_\mathrm{c}$ is

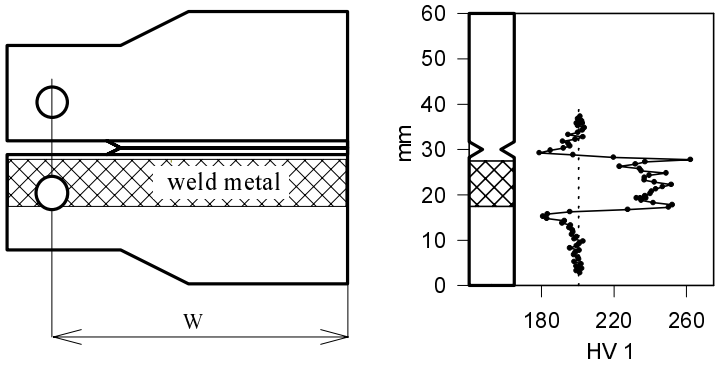

Fig. 1. The weldment in the sidegrooved TDCB – sample, $W = 65$ mm.

the displacement rate in the line of load due to creep. In order to obtain a calibrated relationship, the limit analysis approximation is assumed. C^* can be then expressed as follows [10]:

$$C^* = \frac{n}{n+1}\eta\left(\frac{a}{W}\right)\frac{P\dot{\Delta}_{\mathrm{c}}}{(W-a)B_{\mathrm{net}}}, \tag{4}$$

where a is the crack length, B_{net} is the thickness of the specimen between the grooves and the function $\eta(x)$ is derived from the constraint function g that enters the limit load:

$$\frac{P_y}{\sigma_y} = g\left(\frac{a}{W}\right)WB_{\mathrm{net}}, \quad \eta(x) = -(1-x)\frac{g'}{g}, \tag{5}$$

prime denotes the derivative. For the limit load of the CT sample, it is [11]

$$g(x) = \sqrt{(1+b)(1+bx^2)} - bx - 1, \tag{6}$$

where $b = 1$ and 1.702041 for plane stress and plane strain, respectively.

The constants n and A of the power law (2) for the intercritical layer were estimated on the base of rupture times of the weldment [12], supposing the similitude between Monkman-Grant product $\dot{\varepsilon}_{\mathrm{s}}t_{\mathrm{f}}$ both for the base and for the intercritical structure. At 600 ℃, it is $n = 13.2$, $A = 1.3 \times 10^{-37}$ $\mathrm{s}^{-1}\cdot\mathrm{MPa}^{-n}$ for the base material and $n_{\mathrm{w}} = 10.9$, $A_{\mathrm{w}} = 6.9 \times 10^{-32}$ MPa^{-n} for the weldment.

The line displacement due to creep, which enters in Eq. (4), would be accessible from the permanent displacement provided a correction on instantaneous plasticity was involved. The "immediate" increment of plastic strain due to a change in the

flow stress is related to work hardening. The creep strain, on the other hand, is governed primarily by recovery processes and it depends continuously on the stress. For constant load tests, the optional contribution of immediate plasticity to the overall displacement rate is connected with an increase of the net stress on the bearing ligament as a consequence of crack growth. Provided the plastic deformation were small enough in comparison to the creep one [13], the respective contributions $\dot{\Delta}_\mathrm{p}$ and $\dot{\Delta}_\mathrm{c}$ to the total displacement rate

$$\dot{\Delta} = \dot{\Delta}_\mathrm{p} + \dot{\Delta}_\mathrm{c} \tag{7}$$

should be governed by the load and the geometry in the same manner as in pure plastic and pure viscous cases, respectively.

Assuming the extended (i.e. large scale) plasticity and the work hardening power law, its uniaxial form reads

$$\varepsilon_\mathrm{p} = D\sigma^m, \tag{8}$$

the scaling relations give obviously

$$\Delta_\mathrm{p} = k\left(\frac{a}{W}\right)P^m \tag{9}$$

with the plastic compliance k. In terms of the latter quantity, the parameter J, that plays the same role in plastic materials as C^* in viscous materials, can be expressed [10] as

$$J = \frac{1}{m+1}\frac{k'}{k}\frac{P\Delta_\mathrm{p}}{B_\mathrm{net}W}, \tag{10}$$

prime denotes the derivative. The time derivative of (9) at constant load in combination with (10) give finally the anticipated proportionality between the line displacement rate due to immediate plasticity and the rate of crack growth:

$$\dot{\Delta}_\mathrm{p} = (m+1)\frac{JB_\mathrm{net}}{P}\dot{a}. \tag{11}$$

In order to obtain the most consistent fractions of plastic and creep line rates, the parameters J and C^* in expressions (11) and (4) will be calibrated identically according to the well-known [14] approximation of reference stress. For J, it gives

$$J \cong D\sigma_\mathrm{ref}^{m-1}K^2\ ; \tag{12}$$

a similar relation for C^* may be easily obtained. The stress intensity factor is calibrated by $K = f\left(\frac{a}{W}\right)(B_0B_\mathrm{net}W)^{-1/2}P$ where B_0 is the basic (out of grooves)

thickness of the specimen. The reference stress is related to the formerly introduced (5) constraint function $g\left(\frac{a}{W}\right)$ for the limit yielding: $\sigma_{\mathrm{ref}} \equiv P\sigma_y/P_y = P/(B_{\mathrm{net}}Wg)$. Then,

$$\dot{\Delta}_{\mathrm{p}} : \dot{\Delta}_{\mathrm{c}} = \\ = (m+1)D\left(\frac{P}{B_{\mathrm{net}}Wg\left(\frac{a}{W}\right)}\right)^m \dot{a} : \frac{(n+1)\left(1-\frac{a}{W}\right)}{n\eta\left(\frac{a}{W}\right)}A\left(\frac{P}{B_{\mathrm{net}}Wg\left(\frac{a}{W}\right)}\right)^n W \tag{13}$$

will be used, together with (7), to draw the line rate due to creep from the measured rate of permanent line displacement.

In order to estimate the hardening parameters m and D, some tensile tests were carried out at 600 ℃ and several applied rates. Following the superposition of the laws (2) and (8), the total unidirectional plastic strain rate is expressed as

$$\dot{\varepsilon} = mD\sigma^{m-1}\dot{\sigma} + A\sigma^n. \tag{14}$$

The first term corresponds to the instantaneous work hardening, as can be seen by integrating over an infinitesimal interval around an enforced jump of stress. According to (14), the tensile work hardening curves are to be fitted with respect to the four parameters. The actual true plastic rates should be considered.

The results of simultaneous fits for two applied rates are presented in Fig. 2, the saturated stresses based on pure creep experiments being also shown. The parameters n^*, A^* appear to be fairly consistent with the above values of pure creep origin.

3. Creep crack growth results

The creep crack growth data are evaluated and plotted in a conventional representation C^* versus $\dot{a}$, see Fig. 3. In order to calculate the necessary time derivatives most reliably, the data of both permanent line displacement and crack length were fitted using some formerly introduced functions [10]. The line displacement rates due to creep are estimated according to the partitioning relation (13) and using fitted parameters from Fig. 2.

In the late stages of each test, the well-known asymptotic behaviour of power law type

$$\dot{a} = HC^{*\Phi} \tag{15}$$

is approached, H and Φ are empirical parameters. Transient "tails" preceeding the asymptotic law, if any, are most often of concave type. As to the asymptotic behaviour for large crack sizes concerns, a significant effect of load and/or test

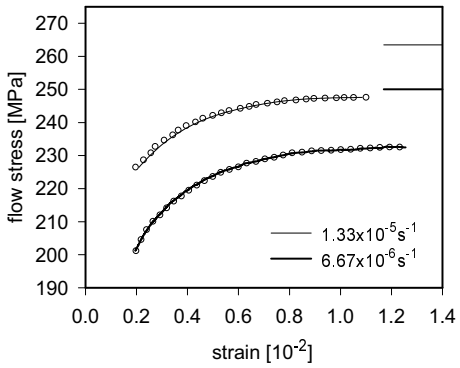

Fig. 2. Fit of tensile data between $\sigma_{0.2}$ and Considere's limit $\sigma = \delta\sigma/\delta\varepsilon$ for steel P91 at 600°C. $n^* = 11.9$, $A^* = 3.93 \times 10^{-34}$ $\mathrm{s^{-1} \cdot MPa^{-n^*}}$, $m = 2.81$, $D = 1.30 \times 10^{-9}$ $\mathrm{MPa^{-m}}$.

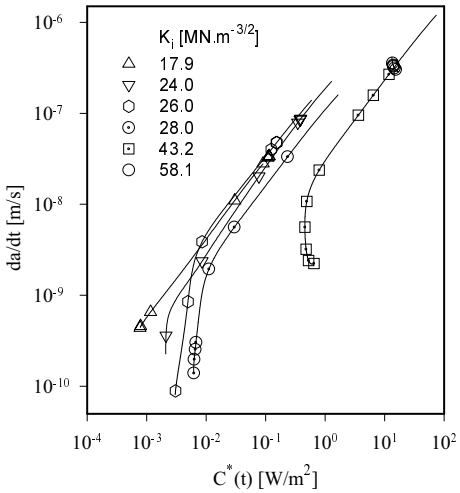

Fig. 3. Creep crack growth rate versus C^* in the intercritical structure for a weldment of parent steel P91.

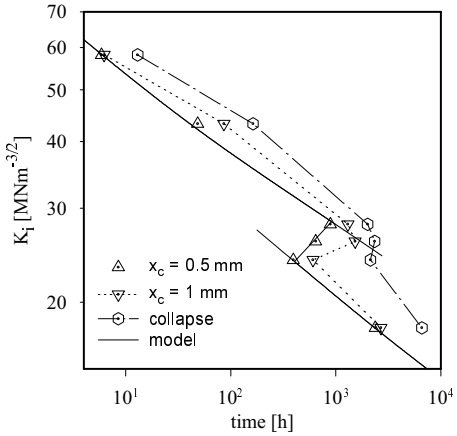

Fig. 4. Times of crack growth initiation in the intercritical structure. Model curves for $n = 6$, $h_1 = 10^{-38}$, $h_2 = 7.8 \times 10^{13}$, $h_3 = 8 \times 10^{50}$ (in SI), $\varepsilon_\mathrm{f} = 1$ and $1/3$ for the upper and lower normal regime, respectively.

time has been detected. For higher loads, when the test (collapse) times remain short enough, the growth rates of large cracks are almost one order of magnitude lower in comparison to the growth rates for long term tests and the same C^*. This behaviour is quite similar to that formerly observed for the base material [10]. In the latter case, however, a still more pronounced influence of thermomechanical exposure on the crack growth has been detected.

In order to obtain maximum possible information about the effect of thermomechanical exposure, the initiation times for the start of crack growth were evaluated. These periods are conventionally defined [15] by a critical increment x_c of the crack length with respect to its initial value. In our case, the critical lengths 0.5 and 1 mm were chosen and the respective times were determined with help of the analytical fits of the measured data: time vs. crack length.

Both initiation times together with the collapse time (lifetime) are plotted against the initial stress intensity factor in Fig. 4. The normal course of initiation time decrease with increasing load is interrupted by a range of inverse, anomalous regime. A significantly smaller fractional period (cf. the horizontal bandwidth in Fig. 4) of subcritical growth in the upper (short term) normal regime in comparison to the long term normal regime is to be noted. This represents a difference with respect to the base material, when stage of the subcritical growth in the upper normal regime vanishes practically, and the creep of continuous sample is followed immediately by a sudden fracture.

4. Discussion

The process of crack growth in viscous materials is likely to be similar but not quite identical as the creep failure. Unlike in the common creep, the damage mechanisms such as nucleation, growth and coalescence of cavities and linking up of microcracks are developed under strongly varying multiaxial stress state. Supposing the increment of crack length is related to the achievement of a critical strain ε_f at the crack tip, the crack rate is approximately given by [5]

$$\dot{a} = \frac{\pi c_n}{\varepsilon_f} \sin^{-1} \frac{\pi n}{n+1} \left[A(a-a_0)\right]^{1/n+1} \left[C(t)\right]^{n/(n+1)}, \tag{16}$$

where c_n combines numerical constants of HRR solution. The true parameter of crack tip fields, $C(t)$, can be assumed as the quantity $C^*(t)$ given by (4) except a very small scale of creeping zone [13]. The root factor $(a-a_0)^{1/(n+1)}$ reflects approximately the effect of the strain gradient ahead of the crack tip. In very early stages of crack growth, irrespective of the actual size of creep zone, the crack growth rate is reduced due to a high strain gradient with respect to the power law (15). In late stages, however, the root factor in (16) is rather insensitive to the crack length, and the asymptotic growth law is approached, not being connected necessarily with the full extended creep.

An exhibition of the just outlined drop of propagation velocity in an extremely steep strain gradient is represented by various forms of initial transients in Fig. 3. According to [16], this effect can lower the crack growth rate in materials with $n = 10$ up to one order of magnitude with respect to the back-extrapolated asymptotic value.

In accordance with relation (3), the crack growth rate is proportional directly to the creep strain rate and inversely to ductility, all the material effect at given geometry being comprised in the creep fracture time. In the common crack growth representation, however, the creep strain rate determines the level of C^*, whereas the variability of crack rate at fixed C^* should be almost purely given by ductility. This follows from relation (16), assuming here only a slight strain rate dependence due to a high root of the parameter A. Therefore the increase of the crack growth rate in a slow creep cracking process, which was observed both for parent material [10] and for the intercritical zone, appears to be related to a decrease in ductility.

Examples of fracture surfaces as left by passage of crack through the critical structure in the slow and fast regimes are given in Figs. 5a and 5b, respectively. The marked difference in the density of dimples is qualitatively the same as documented previously for the parent material, too. Supposing the array of dimples is correlated to the developed overcritical cavities, some kind of continuous cavity nucleation is obvious rather than a constant density of cavities, perhaps nucleated immediately upon application of load. If the cavity accumulation rate N_ε were steady during the creeping, the surface density of dimples would be proportional to $N_\mathrm{f} = N_\varepsilon \varepsilon_\mathrm{f}$. By drawing an empirical law $\varepsilon_\mathrm{f} N_\varepsilon^{2/5} \approx \mathrm{const}$ from [17] which is met for a rather wide group of engineering materials, N_f may be rewritten as

$$N_\mathrm{f} \approx \mathrm{const} \cdot N_\varepsilon^{3/5}. \tag{17}$$

Thus, the accumulation rate of cavities appears to be greater for slow cracking process.

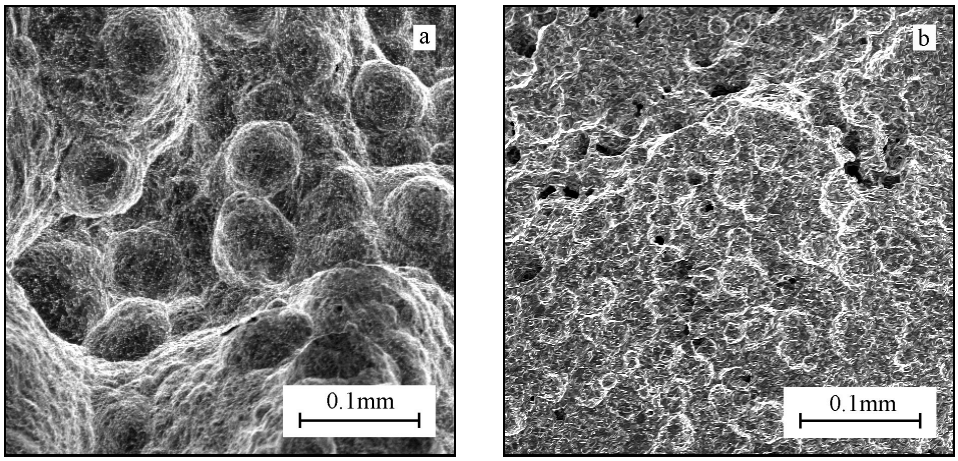

Fig. 5. SEM of fracture surfaces after passage of crack in intercritical structure at 600 °C, crack propagation downward. a) fast test, $K_\mathrm{i} = 58.1\ \mathrm{MN \cdot m^{-3/2}}$, collapse time 19 h, b) slow test, $K_\mathrm{i} = 17.9\ \mathrm{MN \cdot m^{-3/2}}$, collapse time 6603 h.

Cavities are usually assumed to nucleate by clustering of vacancies or by thermally activated breaks of atomic bonds. The necessary large stress concentrations can be created at second phase particles at normally loaded or sliding grain boundaries, at the intersections of slip bands with grain boundary particles or at grain boundary triple points and ledges. Commercial materials usually contain many second-phase particles at grain boundaries which minimize grain boundary sliding [5]. These particles are the most frequent cavity nucleation sites.

Cavities formed must be sufficiently large that they do not shrink due to surface energy γ. Under the local tensile stress σ_{n}, the over-critical cavity sizes are given by $r > 2\gamma/\sigma_n$. Even though the concentration of normal stress is sufficient for nucleation, growing cavities are formed only for relatively large initial decohesions. Hence, the importance of grain boundary sliding for cavity nucleation follows, especially on the grain boundaries inclined to the direction of maximum principal stress.

Assuming the above considerations, the accumulation rate of cavities is suggested as $N_\varepsilon = c_{\mathrm{gb}}/\varepsilon_{\mathrm{c}}$, where c_{gb} is the surface concentration of the still cavity free second-phase particles and ε_{c} is the mean cavitation strain to produce a stable cavity at one particle. The value of ε_{c} depends on γ, σ_{n} and also on the efficiency of grain boundary sliding to produce critical decohesions. To fit the experimental situation of effectively constant accumulation rate, a sufficiently large cavitation strain $\varepsilon_{\mathrm{c}} \geq \varepsilon_{\mathrm{f}}$ must be assumed to exclude an influence of saturation on nucleation rate. Consistently, the concentration of nucleation sites c_{gb} is to identify with its initial value which equals the density c_{gbp} of grain boundary particles.

In order to estimate the strain to rupture, we combined the continuous nucleation of cavities with their diffusive growth under creep constraint. At these conditions, diffusive fluxes responsible for the cavity growth cannot be matched with the overall creep deformation rate without relaxing the maximum normal stresses on the cavitating facet. According to [5], most tests (i.e. not extremely fast) on commercial alloys are carried out within this regime. The corresponding rate of cavity growth $\dot{r}$ is governed by the overall creep strain rate $\dot{\varepsilon}$. Using a simplified expression [18], $\dot{r} = \dot{\varepsilon} d\lambda^2/(4\pi r^2)$, where d is the size of cavitating facet and λ is the instant spacing of cavities, the following relationship can be obtained:

$$\varepsilon_{\mathrm{f}} = \frac{1}{\Gamma\left(\frac{2}{3}\right)} \left(\frac{6\varepsilon_{\mathrm{c}}}{\pi d^2 c_{\mathrm{gbp}}} \right)^{1/3}, \tag{18}$$

where Γ is the Gamma function. This relation should involve all microphysical factorization of the ductility including its inverse proportionality to the density of grain boundary particles. Since in our case the accumulation of cavities appears to be controlled rather by strain than by time [17], the independent nucleation strain ε_{c} on external stress at constant structure can be expected. The expression

(18) then corresponds to Monkman-Grant rule, the variances in ductility being related to changes in the density c_{gbp} of grain boundary particles and possibly to a dependence of ε_{c} on the surface energy via the critical size of cavity.

The nucleation time will be estimated from the requirement that the local strain at a nucleation distance x_{n} ahead of the initial crack tip position just reaches the value of the ductility, ε_{f}. In the limit of small scale creep after the beginning of loading, the asymptotic stress field is, similarly as in the case of extended creep, of the HRR-type, but with the time dependent amplitude [5] $C(t) = \kappa K^2/(n+1)Et$. Here $\kappa = 1$ and $1-\nu^2$ for plane stress and plane strain, respectively, E and ν have their usual meaning. In the long time limit, the field amplitude $C(t)$ must approach the asymptotic steady state value C^*. Either limiting expression for stress gives clearly a negligible contribution in the opposite limit. Consequently, the strain rate in the transient regime will be interpolated by the sum of the creep rates as calculated from the power law (2) and either limiting stress field. The equivalent strain rate at a distance r ahead of the crack tip then reads

$$\dot{\varepsilon}_{\mathrm{eq}} = c_{\mathrm{n}} A^{1/(n+1)} r^{-1/(n+1)} \left[\left(\frac{\kappa K^2}{(n+1)Et} \right)^{n/(n+1)} + C^{*n/(n+1)} \right] . \qquad (19)$$

Inserting $r = x_{\mathrm{n}}$ and integrating up to the strain ε_{f}, the instant t_{n} of crack growth nucleation is obtained.

The initiation time t_{i} comprises further the time for the crack increment to attain the critical value x_{c}: $t_{\mathrm{i}} = t_{\mathrm{n}} + x_{\mathrm{c}}/\dot{a}$. Provided the crack growth rate is given by (16) with the asymptotic C^* and using the approximation of reference stress (12), a relation between initial stress intensity factor K_{i} and initiation time follows. The influence of ductility can be manifested by the formula

$$(h_2 \varepsilon_{\mathrm{f}} - h_1 K_{\mathrm{i}}^n t_{\mathrm{i}})^{n+1} = (n+1) K_{\mathrm{i}}^n \left(K_{\mathrm{i}}^n t_{\mathrm{i}} - h_3 \varepsilon_{\mathrm{f}} \right) . \qquad (20)$$

The coefficients h_{i} depend on nucleation and critical crack lengths, actual geometry and material parameters E, A, and n.

The effect of reduction in ductility is visualised by the calculated curves in Fig. 4. Due to the lack of some input parameters, the h_{i} coefficients could not be calculated directly. Instead, they have been estimated to nearly fit the $K_{\mathrm{i}} - t_{\mathrm{i}}$ data. Note, that the drop in ductility for long term tests appears to be governed by the load. Consequently, the assumed service degradation of structure due to precipitation should be prevented under conditions of high creep rates.

The proposed relation between long term thermomechanical exposition under low load and additional precipitation is documented by transmission electron micrographs in Figs. 6a,b. Due to the corresponding drop in ductility, an increase in creep crack growth rate occurs. This kind of mechanical degradation must be considered when welded components for long service times are designed.

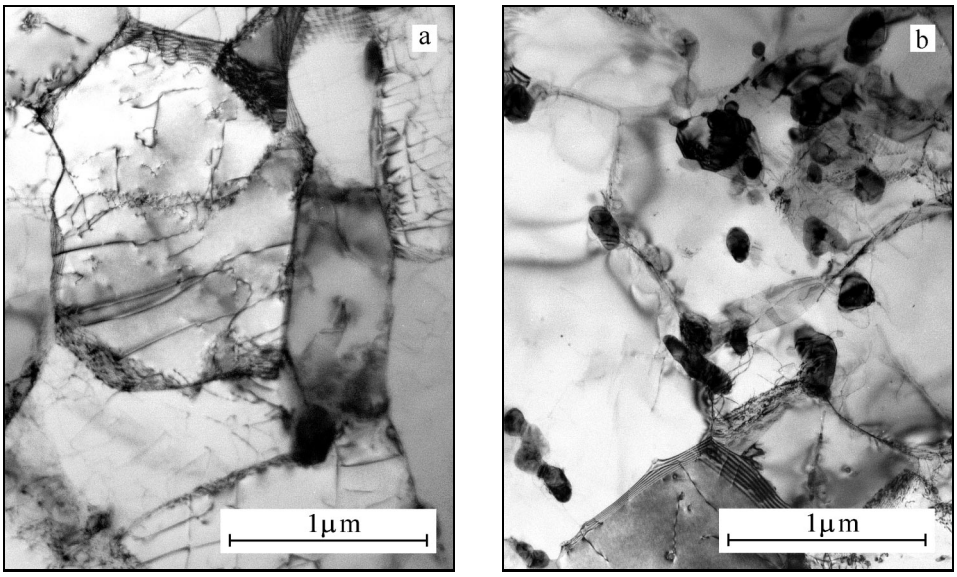

Fig. 6. TEM of exposed intercritical structures ahead of the crack tip, 600 °C. a) fast test, $K_i = 58.1$ MN·m$^{-3/2}$, exposition time 19 h, b) slow test, $K_i = 17.9$ MN·m$^{-3/2}$, exposition time 6603 h.

5. Conclusion

The creep crack growth in the intercritical layer at HAZ for welded steel P91 is affected by test time in a similar manner as in base material. The asymptotic rate of crack growth is appreciably higher for long term tests than for short term tests at the same C^*. A range of inverse dependence of crack initiation time on load is also observed. These effects indicate that a non-constant fracture strain is established under different load and creep rate conditions. A structure degradation due to continuous re-precipitation during long term tests is proposed to cause a drop in ductility and, consequently, to decrease the crack growth resistance.

Acknowledgements

The authors would like to dedicate this paper to Prof. Dr. Petr Kratochvíl, DrSc., on the occasion of his 70th birthday. The work was supported by the Ministry of Education of Czech Republic in frame of the contract No. 522.20 (COST 522).

REFERENCES

[1] BHADESHIA, H. K. D. H.: ISIJ International, *41*, 2001, p. 626.
[2] ASHBY, M. F.—GANDHI, C.—TAPLIN, D. M. R.: Acta Met., *27*, 1979, p. 699.

[3] HALD, J.: In: Advanced Crep Data for Plant Design & Life Extension (Proc. of Int Seminar). Praha, SVÚM 2003, p. 58.
[4] STRANG, A.—VODAREK, V.: Mater. Sci. Techn., *12*, 1996, p. 552.
[5] RIEDEL, H.: Fracture at High Temperatures. Berlin, Heidelberg, Springer-Verlag 1987.
[6] KUMAR, V.—GERMAN, M. D.—SHIH, C. F.: An engineering approach for elastic-plastic fracture analysis. EPRI Rep NP-1931, Palo Alto (CA), Electric Power Research Institute 1981.
[7] SU, X. W.—ZHU, S. J.—LI, X. H.—WANG, L.—WANG, F. G.: Mater. High Temp., *10*, 1992, p. 251.
[8] KIMMINS, S. T.—SMITH, D. J.: J. Strain Analysis, *33*, 1998, p. 195.
[9] LAHA, K.—CHANDRAVATHI, K. S.—BHANU SANKARA RAO, K.—MANNAN, S. L.—SASTRY, D. H.: Trans. Indian Inst. Met., *53*, 2000, p. 217.
[10] BALÍK, J.—JANEČEK, M.—HAKL, J.: Kovove Mater., *40*, 2002, p. 307.
[11] MILLER, A. G.: Int. J. Press. Vess. Piping, *32*, 1988, p. 197.
[12] JAKOBOVÁ, A.—HENNHOFER, K.—FOLDYNA, V.: In: 20. Vortragveranstaltung Langzeitverfahren warmfester Stähle und Hochtemperaturwerkstoffe. Düsseldorf, VDEh 1997, p. 174.
[13] SAXENA, A.: Mater. High Temp., *10*, 1992, p. 79.
[14] AINSWORTH, R. A.—BUDDEN, P. J.: Fatigue Fract. Engng Mater. Struct., *13*, 1990, p. 263.
[15] HOLDSWORTH, S. R.: Mater. High Temp., *10*, 1992, p. 127.
[16] WEBSTER, G. A.: Mater. High Temp., *10*, 1992, p. 74.
[17] DYSON, B. F.: Scripta Metall., *17*, 1983, p. 31.
[18] HALES, R.: Fatigue Fract. Engng Mater. Struct., *17*, 1994, p. 579.

Received: 19.4.2004